Nanoscale Horizons

ROYAL SOCIETY OF CHEMISTRY

COMMUNICATION

View Article Online
View Journal | View Issue

Cite this: *Nanoscale Horiz.*, 2024, 9, 465

Received 8th November 2023,
Accepted 3rd January 2024

DOI: 10.1039/d3nh00495c

rsc.li/nanoscale-horizons

Phenethylammonium bromide interlayer for high-performance red quantum-dot light emitting diodes†

Qiyin Chen, [ab] Yun Hu,[c] Jie Lin, [c] Jingsong Huang,*[c] Shu-Ling Gong *[a] and Guohua Xie *[ab]

Interfacial modification is vital to boost the performance of colloidal quantum-dot light-emitting diodes (QLEDs). We introduce phenethylammonium bromide (PEABr) as an interlayer to reduce the trap states and exciton quenching at the interface between the emitting layer (EML) with CdSe/ZnS quantum-dots and the electron transport layer (ETL) with ZnMgO. The presence of PEABr separates the EML and the ETL and thus passivates the surface traps of ZnMgO. Moreover, the interfacial modification also alleviates electron injection, leading to more improved carrier injection balance. Consequently, the external quantum efficiency of the PEABr-based red QLED reached 27.6%, which outperformed those of the previously reported devices. Our results indicate that the halide ion salts are promising to balance charge carrier injection and reduce exciton quenching in the QLEDs.

New concepts

Quantum-dot light-emitting diodes (QLEDs) possess high efficiency, high brightness, and wide color gamut, which makes them one of the most promising candidates for active matrix displays. Normally, the hole transporting layer, the emitting layer, and the electron transporting layer are consecutively solution-processed to construct QLEDs. Nevertheless, it is tricky to maximize the electroluminescent performance due to charge imbalance and interfacial defects in the solution-processed devices. In this communication, we managed to passivate the interface between the quantum-dot emitting layer and the commonly used electron transporting layer ZnMgO by introducing phenethylammonium bromide (PEABr), which is one of the ingredients used in perovskite LEDs and solar cells. Based on all-spin-coating procedures, the trap density was significantly reduced from 1.1×10^{18} cm^{-3} (control device) to 5.9×10^{17} cm^{-3}. More importantly, the charge balance was improved simultaneously, resulting in the record high external quantum efficiency of 27.6%, and the considerably low turn-on voltage of only 1.8 V.

Introduction

Colloidal quantum-dot light-emitting diodes (QLEDs), as one of the most promising display technologies, have made considerable advancements in recent years due to their unique properties, *e.g.*, solution processing, high brightness, and wide color gamuts.[1–3] Compared with ZnO, ZnMgO exhibits the lower defects and the well-matched energy level with the emissive layer. Therefore, it has been widely used as the preferred electron transport layer (ETL) in QLEDs due to the high electron mobility, effective hole blocking ability, excellent optical transparency, and favorable band energy levels.[4–6] However, it has been reported that the interface between the ZnO- or ZnMgO-based ETL and the quantum-dot (QD)-based emitting layer (EML) suffers from serious interactions.[7–9] The interface interaction mechanisms can be classified as two major types. The first one is the low conduction band barrier between ZnMgO and QDs, which leads to charge transfer and excessive electron accumulation at the interface. The electron accumulation mainly originates from the imbalanced charge injection due to the huge mobility difference between organic hole transport materials and the ZnO- or ZnMgO-based ETL.[8] The other one is subject to the energy transfer from QDs to the ZnO-based NPs due to the surface traps on QDs and the ZnO-based NPs.[9] Consequently, the interactions frequently induce severe exciton quenching and traps-assisted non-radiative recombination in QLEDs, which limits the electroluminescence (EL) performance.[10,11] In addition, the electron mobility of the ZnO-based ETL is much higher than the hole mobility of the commonly used hole transport materials based on the conjugated polymers. This might cause serious carrier injection imbalance in QLEDs during operation and thus profoundly impair the device efficiency and stability.[12–14]

[a] *Sauvage Center for Molecular Sciences, Hubei Key Lab on Organic and Polymeric Optoelectronic Materials, Department of Chemistry, Wuhan University, Wuhan 430072, China. E-mail: gongsl@whu.edu.cn, ifeghxie@xmu.edu.cn*

[b] *The Institute of Flexible Electronics (Future Technologies), Xiamen University, Xiamen 361005, China*

[c] *Oxford Suzhou Centre for Advanced Research (OSCAR), University of Oxford, Suzhou 215123, China. E-mail: jingsong.huang@oxford-oscar.cn*

† Electronic supplementary information (ESI) available. See DOI: https://doi.org/10.1039/d3nh00495c

In order to address these aforementioned issues related to ZnO, researchers have developed several strategies, including the passivation and chemical doping of the ZnO-based ETL, interfacial modification, device engineering, and ligand modification of QDs.[15–20] Among these strategies, interfacial modification is one of the most cost-effective methods and widely employed in optoelectronic devices, such as organic light-emitting diodes (OLEDs), organic solar cells (OSCs), perovskite light emitting diodes (PeLEDs), and perovskite solar cells (PSCs).[9,21–24] For example, Tang *et al.* modified the interface between the perovskite EML and the ZnMgO ETL with the amino-based compound, which not only interacted with ZnMgO and thereby modified the growth of perovskite film, but also passivated the perovskite defects.[25] Tulus *et al.* fabricated the ZnO-based PSCs with the interlayer C_{60}, which passivated the interfacial trap states and reduced non-radiative recombination losses, resulting in the increased efficiency and stability.[26] Soultati *et al.* inserted a thin organic layer between the ZnO ETL and the photoactive layer in the nonfullerene-based OSCs.[27] It reduced the work function of ZnO, improved the electron transport, and increased the degree of crystallization of the photoactive layer. As a result, the photostability and power conversion efficiency of OSC devices were significantly improved.

Since the universality of interfacial modification has been demonstrated in different ZnO-based optoelectronic devices, many interfacial materials, such as PMMA, PVPy, Al_2O_3, PEIE and Cs_2CO_3, have been introduced into QLEDs to improve the EL performance.[5,28–31] For instance, Dai *et al.* inserted an ultrathin insulating layer PMMA at the ZnO/QDs interface to reduce the interaction between ZnO and QDs, and obtained a high external quantum efficiency (EQE) of 20.5%.[5] Yun *et al.* used the non-conjugated polymer PVPy as the interlayer in the inverted QLEDs to efficiently block the leakage current.[28] Qiu *et al.* fabricated the QLEDs with Cs_2CO_3 to inhibit the interaction between ZnO and QDs and passivate the defects on the surface of QDs. Finally, the current efficiency was improved from 10 to 32 cd A^{-1}.[31]

In this contribution, we introduced a halide ion salt, phenethylammonium bromide (PEABr), as the interfacial modification layer inserted between the CdSe/ZnS-based EML and the ZnMgO ETL. The outstanding EQE of 27.6% was demonstrated, due to the balanced charge carrier injection and reduced exciton quenching. To our knowledge, this is the highest EQE of the CdSe/ZnS-based red QLEDs ever reported. The photoluminescence (PL) and time-resolved photoluminescence (TRPL) results indicated that PEABr could passivate the surface traps of ZnMgO and suppress interfacial exciton quenching, simultaneously. The measurements of the transient electroluminescence (TREL) and the electron-only device (EOD) confirmed the improved balanced carrier injection and the reduced interfacial trap density in the presence of PEABr.

Results and discussion

As shown in Fig. 1a, the transmission electron microscope (TEM) image reveals that the QDs exhibited a uniform monolayer dispersion with an average size of about 14 nm (see Fig. 1b). The QD film exhibited an absorption peak at 617 nm and a PL peak at 624 nm with a full-width at half-maximum (FWHM) of 24 nm. The steady-state PL spectra of QDs, QDs/PEABr, QDs/PEABr/ZnMgO, and QDs/ZnMgO were compared to investigate the influence of PEABr on the fluorescence quenching (see Fig. 1d). The PL intensity of the QDs on quartz is comparable to that of QDs/PEABr. Nevertheless, the sample with QDs/ZnMgO displayed the lowest PL intensity. After inserting PEABr between the QDs and ZnMgO, the exciton quenching was significantly alleviated.

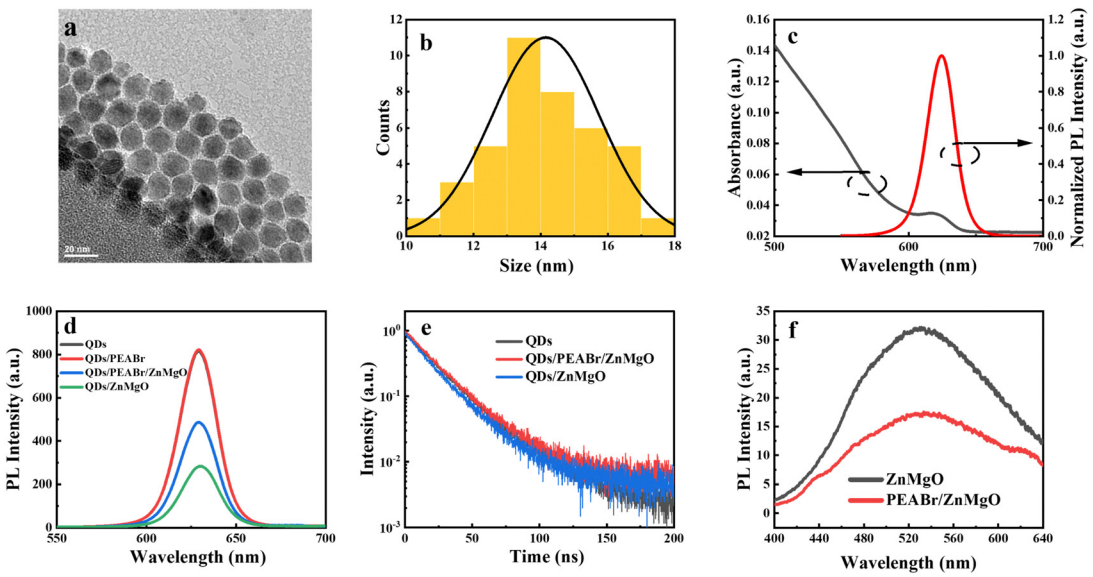

Fig. 1 The TEM image (a) and size distribution (b) of the QDs. (c) Absorption and PL spectra of the red CdSe/ZnS QDs. (d) The PL of the QDs, QDs/PEABr, QDs/PEABr/ZnMgO, and QDs/ZnMgO deposited on quartz, respectively. (e) TRPL of the QDs, QDs/PEABr/ZnMgO, and QDs/ZnMgO, respectively. (f) PL spectra of ZnMgO and PEABr/ZnMgO.

The TRPL was recorded to unravel the role of PEABr. The TRPL spectra of QDs, QDs/PEABr/ZnMgO, and QDs/ZnMgO, shown in Fig. 1e, rendered the average fluorescence lifetimes (τ_{avg}) of 23.8, 22.3 and 20.2 ns, respectively. The τ_{avg} of QDs/PEABr/ZnMgO was longer than that of QDs/ZnMgO, slightly shorter than that of the pristine QDs. The prolonged fluorescence lifetime resulted from the separation of the QDs and ZnMgO. As confirmed by Fig. 1f, the PL intensity of ZnMgO was significantly reduced when ZnMgO was deposited on PEABr. Since the emission of ZnMgO in the visible wavelength range is ascribed to the surface traps,[32–34] it suggests that PEABr can effectively passivate the surface traps of ZnMgO. Combining these PL and TRPL results, it is clear that the fluorescence quenching of the QDs/ZnMgO film was caused by the surface traps of ZnMgO, which can be easily passivated by PEABr.

Fig. S1 (ESI†) presents the atomic force microscopy (AFM) images of the ZnMgO films deposited on the QDs with and without PEABr. Both films displayed comparatively small root mean square (RMS) roughness values of 2.07 and 2.05 nm, respectively. Obviously, the similar RMS values indicate that PEABr has no negative influence on the surface morphologies of ZnMgO.

To evaluate the influence of PEABr on the EL performance of the QLEDs, devices with the structure of anode/hole injection layer (HIL)/hole transport layer (HTL)/EML/interfacial modification layer (IML)/ETL/cathode were constructed, where the anode/cathode were ITO and Al, respectively. PEDOT:PSS, TFB, red emissive CdSe/ZnS QDs, PEABr, and ZnMgO NPs served as the HIL, HTL, EML, IML, and ETL, respectively. The control device without the IML was fabricated in the same run as a reference. The schematic diagram of the PEABr-based device structure is shown in Fig. 2a. Firstly, we compared the EL performance of the devices with different spin-coating speeds, *i.e.*, 1000, 2000, and 3000 rpm, and thereafter two different annealing temperatures (50 °C and 80 °C) of the PEABr layer. The corresponding current density–voltage–luminance (*J*–*V*–*L*), current efficiency (CE), power efficiency (PE), and EQE curves are shown in Fig. S2 and S3 (ESI†) and the key EL paraments are summarized in Tables S1 and S2 (ESI†), respectively.

Later, the optimized fabrication conditions of the PEABr layer were determined with a spin-coating speed of 2000 rpm for 40 s, a fixed acceleration of 1500 rpm, and an annealing temperature of 50 °C for 10 min. In parallel, the corresponding control device was fabricated. The normalized EL spectra of the control and PEABr-based devices under a voltage of 3 V are shown in Fig. 2b. Both devices exhibited identical emission peaking at 628 nm with a narrow FWHM of 24 nm (Table 1). The corresponding to Commission International de I'Eclairage (CIE) color coordinates were (0.68, 0.31). Fig. 2c shows the *J*–*V*–*L* curves of both devices. It is obvious that the current density of the PEABr-based device is lower than that of the control device, which indicates that the presence of PEABr might retard the carrier injection. Also, from the *J*–*V* curves of both devices, we obtained the ideality factor (eqn (1)) by fitting them based on the diode model equation.[35]

$$J = J_0\left[\exp\left(\frac{qV}{nkT}\right) - 1\right] \quad (1)$$

where J is the current density of the diode, V is the voltage of the device, J_0 is the dark saturation current density, q is the elementary charge, n is the ideality factor, k is the Boltzmann constant, and T is the kelvin temperature.

The fitted results reveal that the ideality factor of the PEABr-based device is 4.77. Meanwhile, it is 5.16 for the control one.

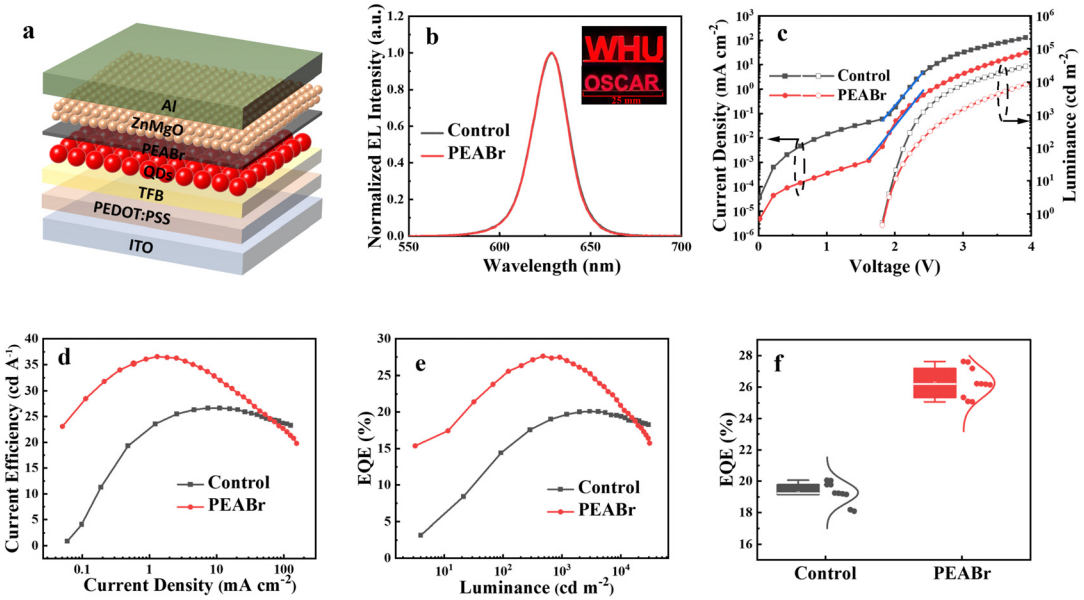

Fig. 2 (a) Schematic diagram of the PEABr-based device structure. (b) Normalized EL spectra. Inset: Photo of two operating PEABr-based QLEDs with different logos. (c) *J*–*V*–*L*, (d) CE, and (e) EQE curves of the device with and without PEABr. (f) Numerical distributions of the EQEs measured from 10 devices, respectively.

Table 1 Comparison of the EL performance of the QLEDs with and without PEABr

Device	V_{on}[a] (V)	λ_{EL}[b] (nm)	FWHM[c] (nm)	PE[d] (lm W^{-1})	CE[e] (cd A^{-1})	EQE[f] (%)	CIE[g] (x, y)
Control	1.8	628	24	31.9	26.6	20.1	(0.68,0.31)
PEABr	1.8	628	24	43.9	36.6	27.6	(0.68,0.31)

[a] Turn-on voltage at a luminance of 1 cd m^{-2}. [b] Peak wavelength of the EL spectrum. [c] Full-width at half-maximum of the EL spectrum. [d] Maximum power efficiency. [e] Maximum current efficiency. [f] Maximum external quantum efficiency. [g] Commission International de l'Eclairage color coordinates.

The lower value of the ideality factor evidences the better diode characteristics. Since both devices share the same hole injection, it is supposed that PEABr alleviates the electron injection and results in a more balanced charge injection in the PEABr-based device. Derived from the luminance curves, both devices exhibited a low turn-on voltage of 1.8 V at a luminance of 1 cd m^{-2}. As shown in Fig. 2d and e, the PEABr-based device exhibited a significantly higher CE and EQE, compared with the control device. The PEABr-based device achieved the maximum EQE, PE, and CE of 27.6%, 43.9 lm W^{-1}, and 36.6 cd A^{-1}, respectively. In contrast, these values of the control device were much inferior, *i.e.*, EQE = 20.1%, PE = 31.9 lm W^{-1}, and 26.6 cd A^{-1}, respectively. It is worth noting that the EQE of the PEABr-based device remained much higher than that of the control device over a wide range of luminance, from 100 to *ca.* 20 000 cd m^{-2}. To the best of our knowledge, such EL characteristics of the PEABr-based device outperformed any other CdSe/ZnS-based red QLEDs. A comparison of the state-of-the-art QLEDs is shown in Table 2.[1,2,36–41] In addition, the devices were easily reproduced, evidenced by the EQE distribution shown in Fig. 2f.

To clarify the role of PEABr in modulating the carrier and exciton dynamics, TREL measurements were conducted. Fig. 3a represents the rising part curves of the devices when applying a pulsed voltage of 3 V. Since the devices shared the same HTL, the slightly delayed switch-on of the EL intensity of the device with PEABr might be attributed to the reduced electron injection (see Fig. 3a), driven by a voltage pulse of 3 V. Combining the *J*–*V*–L curves of both devices, we speculate that PEABr preferred to improve the charge carrier balance by alleviating the injection of electrons. Based on the TREL curves shown in Fig. 3b, the decayed lifetime of the control device (4.04 μs) is shorter than that of the PEABr-based device (12.72 μs), which implies that excitons in the control device suffered from more

Table 2 Comparison of the electroluminescent performance of the state-of-the-art CdSe/ZnS-based red QLEDs

Structure	λ_{EL}[a] (nm)	FWHM[b] (nm)	EQE_{con}[c] (%)	EQE_{mod}[d] (%)	Ref.
ITO/PEDOT:PSS/PVK/QD:TAPC/ZnO/Al	628	28	11.8	15.7	36
ITO/ZnO (LZO)/QD/TCTA/NPB/HAT-CN/Ag	621	24	12.6	16.4	37
ITO/rGO/PEDOT:PSS/PVK/QDs/ZnO/Al	630	21	7.9	17.3	40
ITO/PEDOT:PSS/TFB/QDs/ZnO/Al	628	20	14.3	17.4	38
ITO/PEDOT:PSS/TFB/QDs/ZnMgO/Ag	630	N.A.	16.5	19	1
ITO/ZnO/PEIE/QDs/PVK/PEDOT:PSS/Al	624	32	20.7	N.A.	39
ITO/PEDOT:PSS/TFB (PVK, PTAA, and Poly-TPD)/QD/ZnO (ZnMgO)/Ag	618	N.A.	6.5	21.1	2
ITO/PEDOT:PSS/TFB-PVK/QDs/ZnMgO/Ag	628	N.A.	17.6	22.7	41
ITO/PEDOT:PSS/TFB/QDs/PEABr/ZnMgO/Al	628	24	20.1	27.6	This Work

[a] Peak wavelength. [b] Full-width at half-maximum of the EL spectrum. [c] Maximum external quantum efficiency of the control device. [d] Maximum external quantum efficiency of the modified device. N.A.: not available.

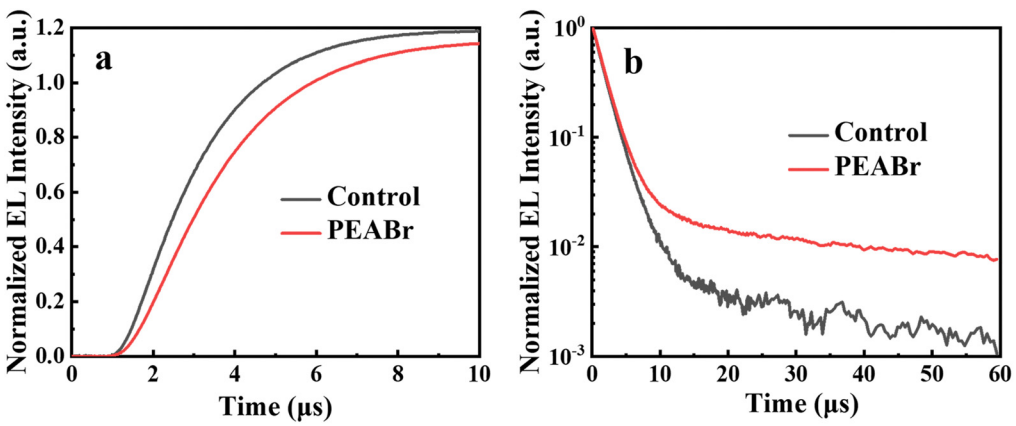

Fig. 3 (a) The rising part, and (b) the decayed part of TREL at a pulsed voltage of 3 V.

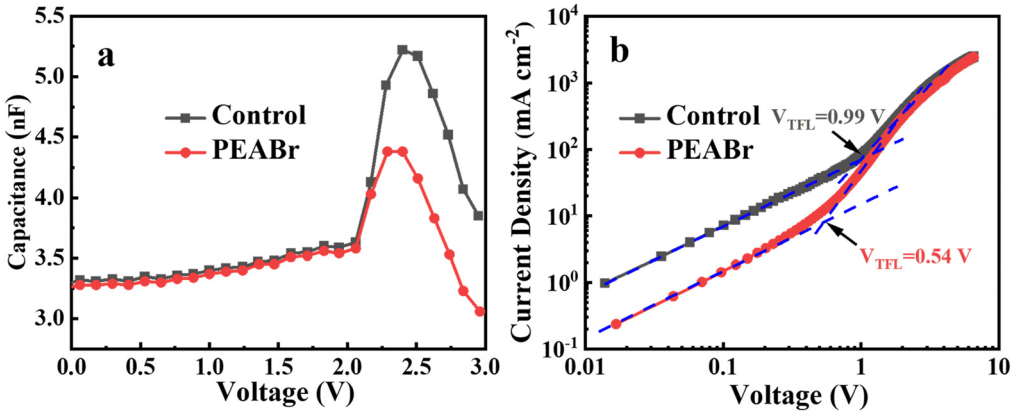

Fig. 4 (a) Capacitance–voltage curves of the control and the PEABr-based QLEDs. (b) *J*–*V* curves of the EODs with and without PEABr.

severe quenching than that in the PEABr-based device. This is well consistent with the TRPL behaviors shown in Fig. 1e.

To further study the effect of PEABr modification on carrier injection, we investigated the capacitance–voltage (*C*–*V*) characteristics of the PEABr-based device and the control one at a fixed frequency of 10 kHz (see Fig. 4a). The geometric capacitance values of both devices are almost constant at 3.3 nF under a low bias voltage <0.5 V. Then the values rise because of the fast carrier injection and decrease significantly after 2.4 V due to the intensive radiative recombination. Since the hole injection would be identical for both devices, the variation of the *C*–*V* curves should be attributed by electron injection. The lower capacitance after the turn-on of the PEABr-based device demonstrates that PEABr reduced the excessive electron injection and decreased the accumulation of electrons in the PEABr-based device. It is clear that the current density of the PEABr-based device was lower than that of the control device while both devices shared the same hole injection (see Fig. 2c). Meanwhile, the *J*–*V* curves of the EODs exhibited the same trend, that the PEABr-based EOD had a lower current density when PEABr was inserted (see Fig. 4b). Furthermore, the similar voltages at the peak capacitance of both devices also indicate that in both devices the built-in potential (V_{bi}) was barely changed, in the presence of PEABr.

The interfacial trap density is an important parameter to manifest the effect of interfacial modification, which can be simply calculated from the *J*–*V* curve of the single-carrier device. Therefore, we fabricated the EODs with the structures of ITO/ZnMgO (60 nm)/QDs (25 nm)/PEABr (5 nm)/ZnMgO (60 nm)/Al (100 nm) (named PEABr-based EOD) and ITO/ZnMgO (60 nm)/QDs (25 nm)/ZnMgO (60 nm)/Al (100 nm) (named control EOD), respectively. Based on the *J*–*V* curves of both EODs shown in Fig. 4b, the intrinsic interfacial trap density (eqn (2)) can be calculated by the following equation.[42]

$$N_t = \frac{2\varepsilon\varepsilon_0 V_{TFL}}{ed^2} \quad (2)$$

where N_t is the intrinsic traps density, ε is the relative dielectric constant of the QDs (6.2), ε_0 is the permittivity of free space, e is the elementary charge, d is the thickness of the device, and V_{TFL} is the trap-filled limit voltage.

The V_{TFL} values were determined to be 0.54 and 0.99 V for the PEABr-based and control EODs, respectively. It is found that the PEABr interlayer reduces the interfacial trap density from 1.1×10^{18} cm^{-3} (control device) to 5.9×10^{17} cm^{-3}. The low N_t mainly originated from the reduced traps passivated by PEABr. This would lead to weaker exciton quenching, which is consistent well with the steady-state PL and TRPL results.

Based on the above-mentioned measurements and characterization, it is deduced that PEABr as the interfacial modification layer not only is beneficial to reduce the trap density and thus suppress exciton quenching, but also helpful to improve carrier injection balance, which plays a vital role in boosting the EL performance.

Conclusions

In summary, state-of-the-art CdSe/ZnS red QLEDs with high reproducibility were successfully demonstrated by introducing PEABr as an interface modification layer. The photophysical and EL experiments clarify that the PEABr layer plays a vital role in suppressing interfacial exciton quenching and improving the charge carrier injection balance, simultaneously. As a result, the PEABr-based device achieved an unprecedentedly high EQE of 27.6% without sacrificing the low turn-on voltage (1.8 V). We believe that understanding the PEABr interlayer will provide a powerful approach to manipulate the EL performance of QLEDs.

Data availability statement

The data that support the findings of this study are available from the corresponding author upon reasonable request.

Conflicts of interest

The authors declare no conflict of interest.

Acknowledgements

This research was financially supported by the National Natural Science Foundation of China (no. 52373195, 62175189 and

61975256). G. X. acknowledges the funding support from the Opening Project of Key Laboratory of Optoelectronic Chemical Materials and Devices, Ministry of Education, Jianghan University (no. JDGD-202301), the Program for Promoting Academic Collaboration and Senior Talent Fostering between China and Canada, Australia, New Zealand, and Latin America (2021-109), and the joint China-Sweden Mobility programme (no. 52211530052). J. H. acknowledges the financial support from the Perovskite Thin-Film Innovation Technology Centre at OSCAR (no. YZCXPT2022104), and the Natural Science Foundation of Jiangsu Province (no. BK20231222). Mesolight (Suzhou) is gratefully acknowledged for providing red CdSe/ZnS QDs and ZnMgO solutions.

References

1 D. Zhao, Y. Zheng, T. Meng, Y. Zhu, J. Jing, X. Chen, H. Gao, C. Mao, W. Zheng, H. Hu, T. Guo and F. Li, Efficient quantum dot light-emitting diodes with ultra-homogeneous and highly ordered quantum dot monolayer, *Sci. China Mater.*, 2022, **65**, 757–763.

2 C. Cheng, X. Sun, Z. Yao, C. Bi, X. Wei, J. Wang and J. Tian, Balancing charge injection in quantum dot light-emitting diodes to achieve high efficiency of over 21%, *Sci. China Mater.*, 2022, **65**, 1882–1889.

3 Q. Chen, Z. Qi, J. Lin, J. Huang and G. Xie, Promise to electrically pumped colloidal quantum dot lasers, *Innovation*, 2023, **4**, 100498.

4 L. Qian, Y. Zheng, J. Xue and P. H. Holloway, Stable and efficient quantum-dot light-emitting diodes based on solution-processed multilayer structures, *Nat. Photonics*, 2011, **5**, 543–548.

5 X. Dai, Z. Zhang, Y. Jin, Y. Niu, H. Cao, X. Liang, L. Chen, J. Wang and X. Peng, Solution-processed, high-performance light-emitting diodes based on quantum dots, *Nature*, 2014, **515**, 96–99.

6 A. Alexandrov, M. Zvaigzne, D. Lypenko, I. Nabiev and P. Samokhvalov, Al-, Ga-, Mg-, or Li-doped zinc oxide nanoparticles as electron transport layers for quantum dot light-emitting diodes, *Sci. Rep.*, 2020, **10**, 7496.

7 B. S. Mashford, M. Stevenson, Z. Popovic, C. Hamilton, Z. Zhou, C. Breen, J. Steckel, V. Bulovic, M. Bawendi, S. Coe-Sullivan and P. T. Kazlas, High-efficiency quantum-dot light-emitting devices with enhanced charge injection, *Nat. Photonics*, 2013, **7**, 407–412.

8 Y. Lee, B. G. Jeong, H. Roh, J. Roh, J. Han, D. C. Lee, W. K. Bae, J.-Y. Kim and C. Lee, Enhanced Lifetime and Efficiency of Red Quantum Dot Light-Emitting Diodes with Y-Doped ZnO Sol–Gel Electron-Transport Layers by Reducing Excess Electron Injection, *Adv. Quantum Technol.*, 2018, **1**, 1700006.

9 J. M. Caruge, J. E. Halpert, V. Wood, V. Bulovic and M. G. Bawendi, Colloidal quantum-dot light-emitting diodes with metal-oxide charge transport layers, *Nat. Photonics*, 2008, **2**, 247–250.

10 J. Kim, D. Hahm, W. K. Bae, H. Lee and J. Kwak, Transient Dynamics of Charges and Excitons in Quantum Dot Light-Emitting Diodes, *Small*, 2022, **18**, 2202290.

11 X. Dai, Y. Deng, X. Peng and Y. Jin, Quantum-Dot Light-Emitting Diodes for Large-Area Displays: Towards the Dawn of Commercialization, *Adv. Mater.*, 2017, **29**, 1607022.

12 H. Chen, K. Ding, L. Fan, W. Liu, R. Zhang, S. Xiang, Q. Zhang and L. Wang, All-Solution-Processed Quantum Dot Light Emitting Diodes Based on Double Hole Transport Layers by Hot Spin-Coating with Highly Efficient and Low Turn-On Voltage, *ACS Appl. Mater. Interfaces*, 2018, **10**, 29076–29082.

13 H. Cho, S. Park, H. Shin, M. Kim, H. Jang, J. Park, J. H. Yang, C. W. Han, J. H. Baek, Y. S. Jung and D. Y. Jeon, Highly Efficient Deep Blue Cd-Free Quantum Dot Light-Emitting Diodes by a p-Type Doped Emissive Layer, *Small*, 2020, **16**, 2002109.

14 S. Chen, W. Cao, T. Liu, S.-W. Tsang, Y. Yang, X. Yan and L. Qian, On the degradation mechanisms of quantum-dot light-emitting diodes, *Nat. Commun.*, 2019, **10**, 765.

15 H.-M. Kim, S. Cho, J. Kim, H. Shin and J. Jang, Li and Mg Co-Doped Zinc Oxide Electron Transporting Layer for Highly Efficient Quantum Dot Light-Emitting Diodes, *ACS Appl. Mater. Interfaces*, 2018, **10**, 24028–24036.

16 D. Liu, S. Cao, S. Wang, H. Wang, W. Dai, B. Zou, J. Zhao and Y. Wang, Highly Stable Red Quantum Dot Light-Emitting Diodes with Long T95 Operation Lifetimes, *J. Phys. Chem. Lett.*, 2020, **11**, 3111–3115.

17 Q. Yuan, T. Wang, P. Yu, H. Zhang, H. Zhang and W. Ji, A review on the electroluminescence properties of quantum-dot light-emitting diodes, *Org. Electron.*, 2021, **90**, 106086.

18 Q. Wan, Z. Li, C. Zhang, W. Zheng, L. Huang, M. Liu, Q. Zhang, B. Wang, W. Liu, L. Kong and L. Li, Surface Oxidation of Quantum Dots to Improve the Device Performance of Quantum Dot Light-Emitting Diodes, *J. Phys. Chem. C*, 2020, **124**, 28424–28430.

19 L. Chen, S. Wang, D. Li, Y. Fang, H. Shen, L. Li and Z. Du, Simultaneous Improvement of Efficiency and Lifetime of Quantum Dot Light-Emitting Diodes with a Bilayer Hole Injection Layer Consisting of PEDOT:PSS and Solution-Processed WO3, *ACS Appl. Mater. Interfaces*, 2018, **10**, 24232–24241.

20 J.-Y. Dong, K. W. Ng, Y.-M. Song, J.-L. Li, Y.-C. Kong, M.-W. Wang, J.-C. Xu, L. Li, S. Chen, Z.-K. Tang and S.-P. Wang, Observation and Suppression of Stacking Interface States in Sandwich-Structured Quantum Dot Light-Emitting Diodes, *ACS Appl. Mater. Interfaces*, 2021, **13**, 56630–56637.

21 Y. Cun, C. Song, H. Zheng, J. Wang, C. Mai, Y. Liu, J. Li, D. Yu, J. Wang, L. Ying, J. Peng and Y. Cao, Modifying the organic/metal interface via solvent vapor annealing to enhance the performance of blue OLEDs, *J. Mater. Chem. C*, 2019, **7**, 4784–4790.

22 G. Xie and K. Leo, Catalyzing n-doping, *Innovation*, 2022, **3**, 100219.

23 Y.-T. Chang, L. Zhang, M.-J. Lai, W.-C. Chiang and L.-C. Chen, High-Performance Quasi-Two-Dimensional $CsPbBr_{2.1}C_{l0.9}$: PEABr Perovskite Sky-Blue LEDs with an Interface Modification Layer, *Nanoscale Res. Lett.*, 2022, **17**, 66.

24 J. Cao, B. Wu, R. Chen, Y. Wu, Y. Hui, B.-W. Mao and N. Zheng, Efficient, Hysteresis-Free, and Stable Perovskite Solar Cells with ZnO as Electron-Transport Layer: Effect of Surface Passivation, *Adv. Mater.*, 2018, **30**, 1705596.

25 L. Tang, J. Qiu, Q. Wei, H. Gu, B. Du, H. Du, W. Hui, Y. Xia, Y. Chen and W. Huang, Enhanced Performance of Perovskite Light-Emitting Diodes via Diamine Interface Modification, *ACS Appl. Mater. Interfaces*, 2019, **11**, 29132–29138.
26 N. Tulus, L. A. Muscarella, Y. Galagan, S. C. Boehme and E. von Hauff, Trap passivation and suppressed electrochemical dynamics in perovskite solar cells with C60 interlayers, *Electrochim. Acta*, 2022, **433**, 141215.
27 A. Soultati, A. Verykios, S. Panagiotakis, K.-K. Armadorou, M. I. Haider, A. Kaltzoglou, C. Drivas, A. Fakharuddin, X. Bao, C. Yang, A. R. B. M. Yusoff, E. K. Evangelou, I. Petsalakis, S. Kennou, P. Falaras, K. Yannakopoulou, G. Pistolis, P. Argitis and M. Vasilopoulou, Suppressing the Photocatalytic Activity of Zinc Oxide Electron-Transport Layer in Nonfullerene Organic Solar Cells with a Pyrene-Bodipy Interlayer, *ACS Appl. Mater. Interfaces*, 2020, **12**, 21961–21973.
28 J. Yun, J. Kim, H.-K. Jang, K. J. Lee, J. H. Seo, B. J. Jung, G. Kim and J. Kwak, Controlling charge balance using nonconjugated polymer interlayer in quantum dot light-emitting diodes, *Org. Electron.*, 2017, **50**, 82–86.
29 Z. Li, Enhanced performance of quantum dots light-emitting diodes: The case of Al_2O_3 electron blocking layer, *Vacuum*, 2017, **137**, 38–41.
30 Y.-L. Shi, F. Liang, Y. Hu, M.-P. Zhuo, X.-D. Wang and L.-S. Liao, High performance blue quantum dot light-emitting diodes employing polyethylenimine ethoxylated as the interfacial modifier, *Nanoscale*, 2017, **9**, 14792–14797.
31 Y. Qiu, Z. Gong, L. Xu, Q. Huang, Z. Yang, B. Ye, Y. Ye, Z. Meng, Z. Zeng, Z. Shen, W. Wu, Y. Zhou, Z. Hong, Z. Cheng, S. Ye, H. Hong, Q. Lan, F. Li, T. Guo and S. Xu, Performance Enhancement of Quantum Dot Light-Emitting Diodes via Surface Modification of the Emitting Layer, *ACS Appl. Nano Mater.*, 2022, **5**, 2962–2972.
32 T. A. Wassner, B. Laumer, S. Maier, A. Laufer, B. K. Meyer, M. Stutzmann and M. Eickhoff, Optical properties and structural characteristics of ZnMgO grown by plasma assisted molecular beam epitaxy, *J. Appl. Phys.*, 2009, **105**, 023505.
33 D. Li, Y. H. Leung, A. B. Djurišić, Z. T. Liu, M. H. Xie, S. L. Shi, S. J. Xu and W. K. Chan, Different origins of visible luminescence in ZnO nanostructures fabricated by the chemical and evaporation methods, *Appl. Phys. Lett.*, 2004, **85**, 1601–1603.
34 P. A. Rodnyi and I. V. Khodyuk, Optical and luminescence properties of zinc oxide (Review), *Opt. Spectrosc.*, 2011, **111**, 776–785.
35 G. J. Wetzelaer and P. Blom, Diffusion-driven currents in organic-semiconductor diodes, *NPG Asia Mater.*, 2014, **6**, e110.
36 H. Liu, J. Zou, X. Zhu, X. Li, H. Ni, Y. Liu, H. Tao, M. Xu, L. Wang and J. Peng, Boosting the performance of solution-processed quantum dots light-emitting diodes by a hybrid emissive layer via doping small molecule hole transport materials into quantum dots, *Org. Electron.*, 2021, **99**, 106344.
37 J. Jing, L. Lin, K. Yang, H. Hu, T. Guo and F. Li, Highly efficient inverted quantum dot light-emitting diodes employing sol-gel derived Li-doped ZnO as electron transport layer, *Org. Electron.*, 2022, **103**, 106466.
38 Y. Li, X. Fan, C. Shen, X. Shi, P. Li, K. N. Hui, J. Fan, K. Kang, T. Zhang and L. Qian, Charge Balance in Red QLEDs for High Efficiency and Stability via Ionic Liquid Doping, *Adv. Funct. Mater.*, 2022, **32**, 2203641.
39 F. Cao, D. Zhao, P. Shen, J. Wu, H. Wang, Q. Wu, F. Wang and X. Yang, High-Efficiency, Solution-Processed White Quantum Dot Light-Emitting Diodes with Serially Stacked Red/Green/Blue Units, *Adv. Opt. Mater.*, 2018, **6**, 1800652.
40 Y. Lei, Y. Zhao, Q. Zhang, Z. Xiong and L. Chen, Highly efficient and bright red quantum dot light-emitting diodes with balanced charge injection, *Org. Electron.*, 2020, **81**, 105683.
41 C. Cheng, A. Liu, G. Ba, I. S. Mukhin, F. Huang, R. M. Islamova, W. C. H. Choy and J. Tian, High-efficiency quantum-dot light-emitting diodes enabled by boosting the hole injection, *J. Mater. Chem. C*, 2022, **10**, 15200–15206.
42 P. Wang, R. Li, B. Chen, F. Hou, J. Zhang, Y. Zhao and X. Zhang, Gradient Energy Alignment Engineering for Planar Perovskite Solar Cells with Efficiency Over 23%, *Adv. Mater.*, 2020, **32**, 1905766.